Development of tools to improve the efficiency of amorphous silicon solar cells

Doctoral Meeting

Montserrat Fortes Ouviña

Centro Singular de Investigación en Tecnoloxías da Información

UNIVERSIDADE DE SANTIAGO DE COMPOSTELA

citius.usc.es

Centro Singular de Investigación en Tecnoloxías da Información

Index

- Introduction
- Objectives
- Solar Cell simulation
  - Set-up
  - Results
  - Conclusions
- Development of VFSR measurement system
  - Set-up
  - Results
  - Conclusions

CiTIUS

Introduction

Photoelectric effect

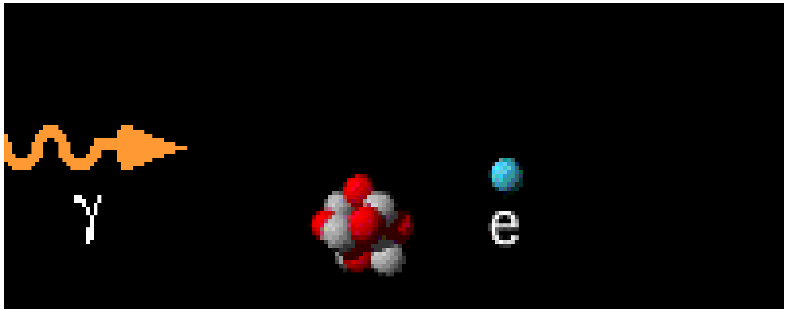

Figure 1: Photoelectric Effect

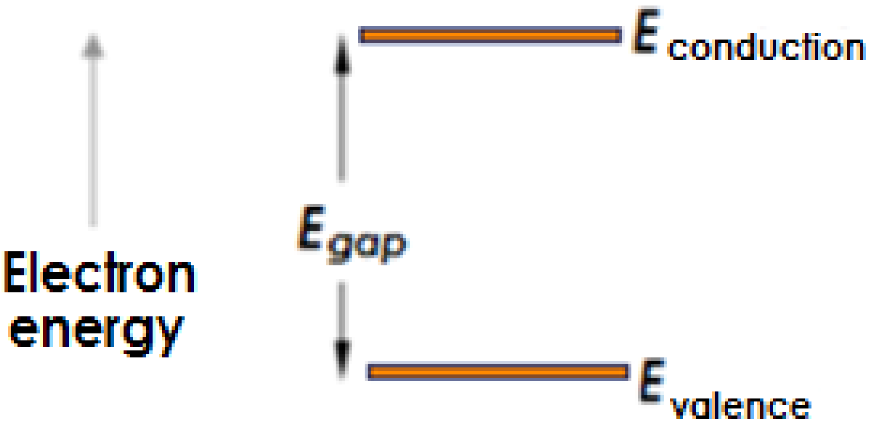

Figure 2: Band Diagram of a Semiconductor

- The transformation of light into electrical energy is based on the photoelectric effect.
- An electric field in the interior of the material can separate them, generating, as they move, electric current.

CiTIUS

Introduction (II)

Cell structure

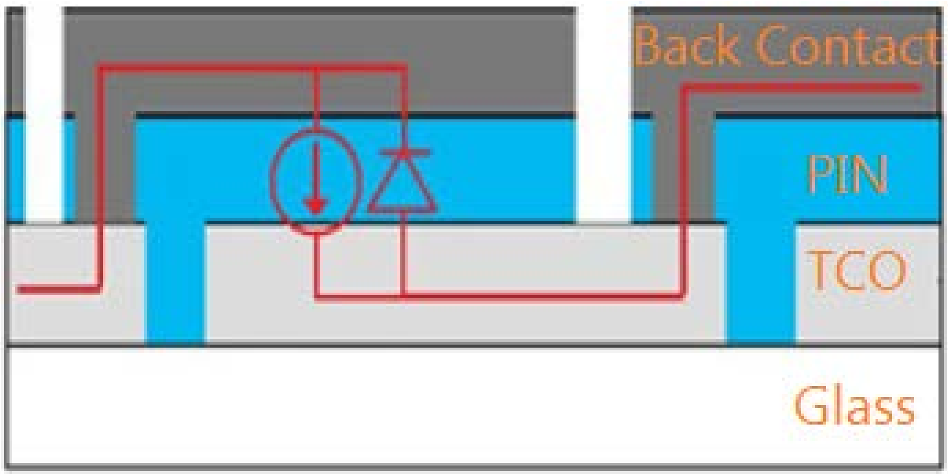

Figure 3: T-Solar a-Si:H Solar Cell structure

- Front contact:
  - Transparent conductive oxide (TCO) deposited on the glass.
  - Texture.
- PIN structure used to induce an electric field:
  - P-type (+) doped layer.
  - Intrinsic layer → Increases the carriers' lifetime.
  - N- type (-) doped layer.
  - PECVD (I and N in the same chamber).
- A back contact:
  - Zinc oxide, aluminum and nickel/vanadium.
  - Reflector.
  - PVD.

CiTIUS

Introduction (III)

PV Module structure

Figure 4: Full modules (5.72 m^2, 216 cells) & Quarter modules (1.43 m^2, 106 cells) in the T-Solar facilities

- Modules' design: Strings of 216 solar cells, width 1 cm connected in series.
- In a series connection: The individual voltages add up while current remains constant.
- The value of the module's current will be limited by the cell generating the less current.

Introduction (IV)

Importance of the uniformity of the layers

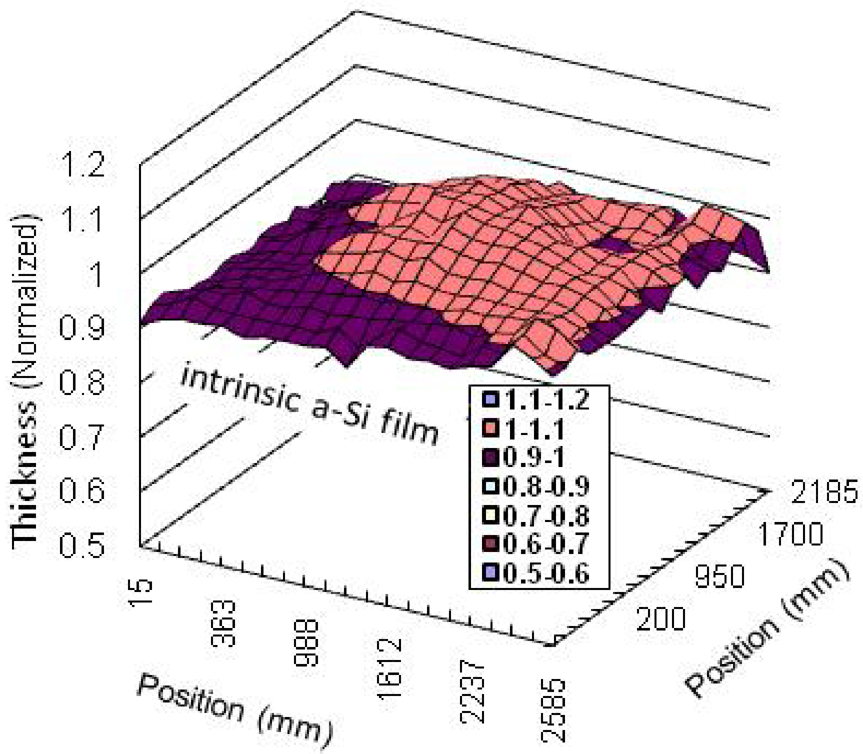

Figure 5: Typical thickness distribution of the intrinsic a-Si:H layer

- Therefore, ↑uniformity in the deposition of the p-i-n layers is necessary to assure very uniform current generation.

- This will be translated into a higher module efficiency.

- In the other hand, the locally generated current (J_{sc}) can be calculated from the SR measurement of a small illuminated area.

CiTIUS

Introduction (V)

Spectral Response

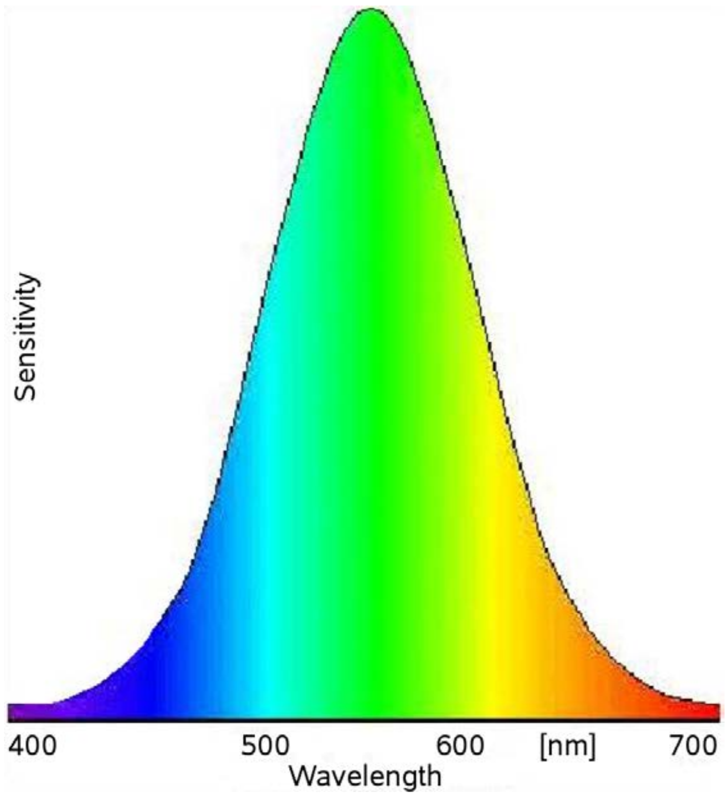

Figure 6: Scheme representing the photosensitivity as function of the incident wavelength

- SR → photosensitivity (R, A/W) measured along the light spectrum.
- R → intensity of the photovoltaic effect depending on the incoming wavelength.
- External Quantum Efficiency (EQE, %) → number of electron/hole pairs generated in the cell by the incident photon flux.
- Both parameters are linked by the following equation:

$$EQE = \frac{R}{q} \cdot \frac{hc}{\lambda} = (1240\,[\mathrm{V} \cdot \mathrm{nm}]) \cdot \left(\frac{\mathrm{R}}{\lambda}\right)$$

CiTIUS

Introduction (VI)

Illumination I-V characteristic

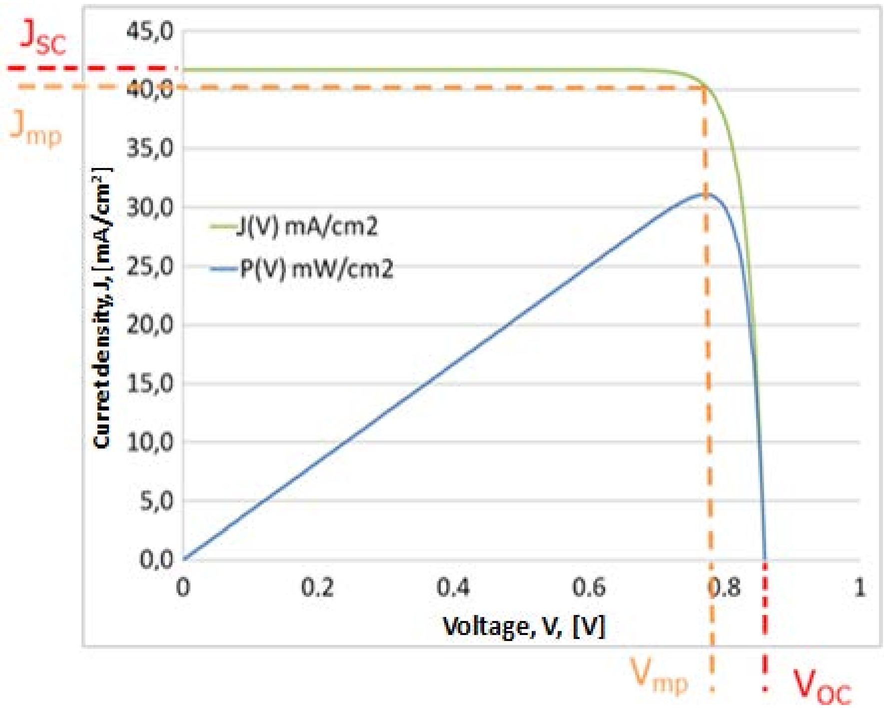

Figure 7: Example of a typical Illumination J-V curve of a solar cell

- I_{SC} → Maximum current (zero load)
  - Proportional to area→ J_{SC} (mA/cm²).
- Open circuit voltage (V_{oc}):
  - Maximum voltage.
  - No current (infinite resistance).
- Max. power density : $P_{mp} = J_{mp} V_{mp}$.
- Fill Factor $$FF = \frac{J_{mp} Vmp}{J_{SC} V_{oc}}$$
- Efficiency $$\eta = \frac{J_{mp} V_{mp}}{P_S}$$

CiTIUS

Introduction (VII)

Equivalent Circuit

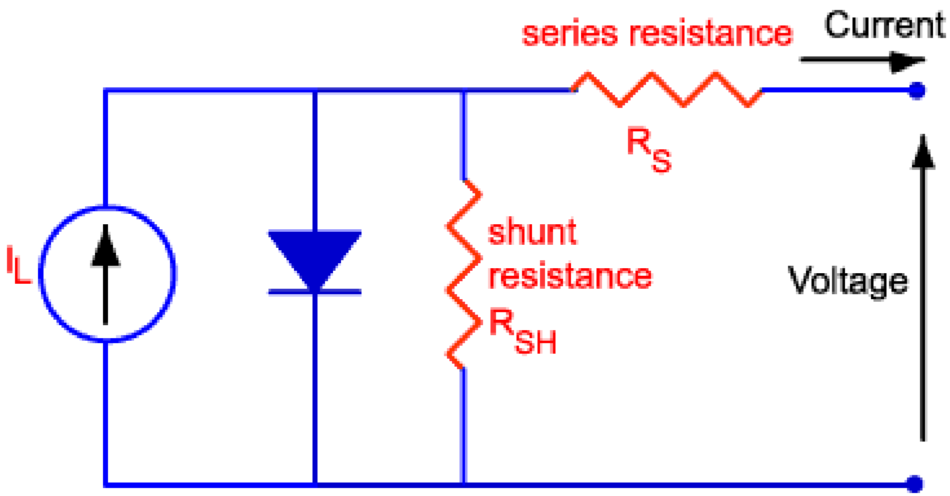

Figure 8: Simplified equivalent circuit of a solar cell with its parasitic defects

- Current source (photogenerated current) in parallel with a diode (pn junction).
- Series resistance:
  - Dominant at low currents.
  - Contact-Semiconductor interface.
- Shunt resistance:
  - Dominant at high currents.
  - Undesired high conductive paths.

CiTIUS

Introduction (VIII)

Effect of Rs and Rsh on the Dark I-V characteristic

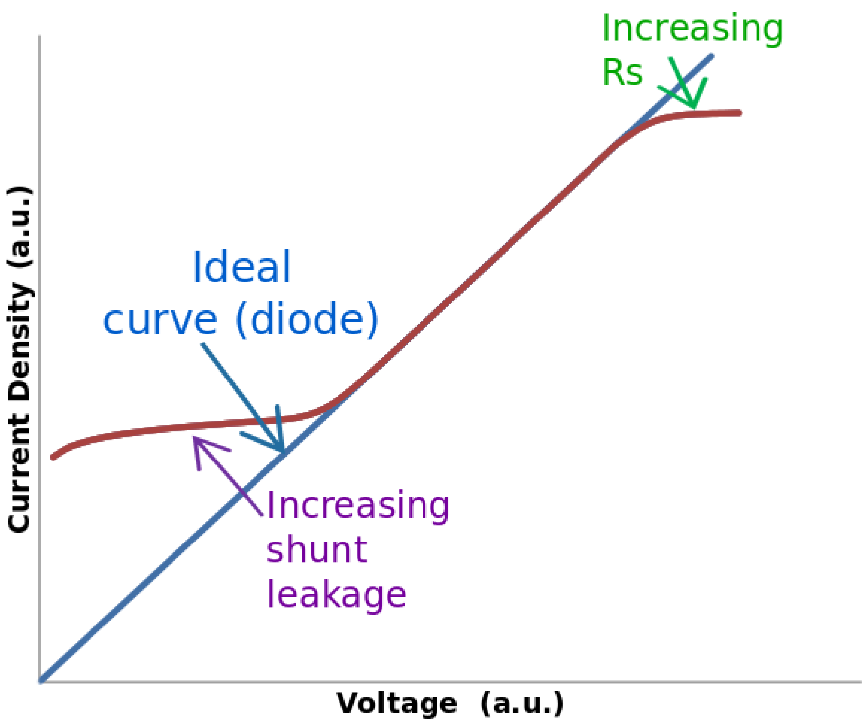

Figure 9: Schematic Dark semi-logarithmic J-V plot of a solar cell, showing the effect of shunt leakage and R_s

- The smaller the shunt resistance, the greater the undesired excess current at low biases.
- On the contrary, increasing R_s limits the current at high voltages.

CiTIUS

Introduction (IX)

Effect of Rs and Rsh on the Illumination I-V characteristic

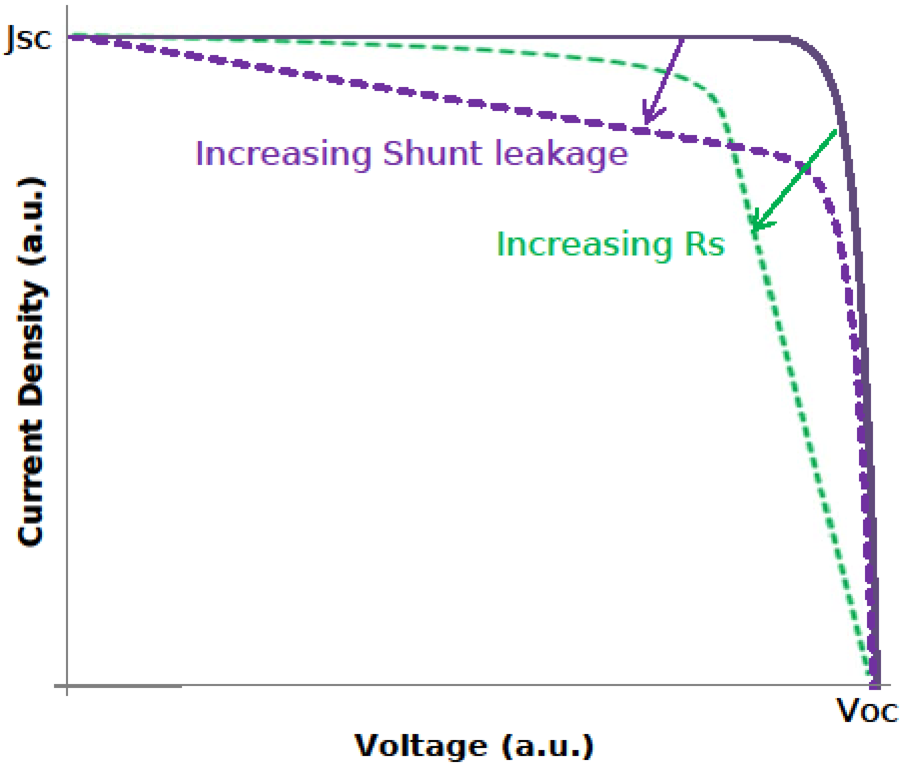

Figure 10: Schematic representation of the effect of increasing shunt leakage and R_s, on the Illumination J-V curve of a solar cell

- ↑ shunt leakage (↓ R_{sh})
  - ↓ currents from 0 V to V_{mpp}.
  - ↓ FF.
- ↑ R_s → ↓ current at biases higher than V_{mpp}.

CiTIUS

Introduction (X)

Staebler Wronski Effect

- Efficiency reduction in the first hours of illumination.
- Creation of new defects (in addition to the initially present dangling bonds) due to the breaking of weak Si–Si bonds.
- The effect stabilizes at arround ≈300 kWh/m^2.
- The stabilized (or degraded) efficiency can be around 10–20% lower than the initial one.
- In a-Si:H technology, the degraded efficiency is indicated as comparison criteria with the rest of PV devices.

CiTIUS

Objectives

GENERAL

- The pursuit of a better performance of thin film amorphous silicon solar cells.

FULLFILLED OBJECTIVES

- Analysis of the impact of the defects present in the device upon the overall efficiency.
- Development of a very fast spectral response measurement system, able to be placed in a production line.

CURRENT WORK

- Simulation of the quantum efficiency of our device using an electromagnetic model.
- Upgrading of VFSR equipment system.

Solar Cell Simulation

Simulation tool and simulated ideal device

Figure 13: Schematic representation of the cross-section of the simulated pin a-Si:H solar cell

- TOOL→ Sentaurus TCAD.
- Experimental data:
  - Optical data of the layers.
  - Idealized a periodic texture based on experimental AFM measurements.
- Modeling of heterojunctions → buffer layers with gradual dopping.
- Modifications to model a-Si:H:
  - Continuous density of states (DOS).
  - Model for recombination-generation rate involving the localized states in the mobility gap of a-Si:H.

CiTIUS

Solar Cell Simulation (II)

Simulation of the parasitic elements

Figure 14: Schematic representation of the simulated pip structure

- Modeling R_s
  - Ohmic resistance in the TCO/p-layer with the experimental value: 3.5 Ω.
- Modeling R_{sh}
  - Complex experimental features:
    - voltage symmetry with V=0
    - power dependence with voltage
    - weak temperature dependence
    - large fluctuation among cells
  - Explanation in literature:
    - Local non-uniformities, such as AZO grain boundaries or areas where Al can diffuse, counter doping n-layer
    - Studies have shown that phosphorus accelerates the Al diffusion
    - Local pip-structures 10^{-4}-10^{-6} smaller than the solar cell
  - $I_{cell}= (J_{cell})(A_{cell})+(J_{pip})(A_{shunt})$

Solar Cell Simulation (III)

Results under dark conditions

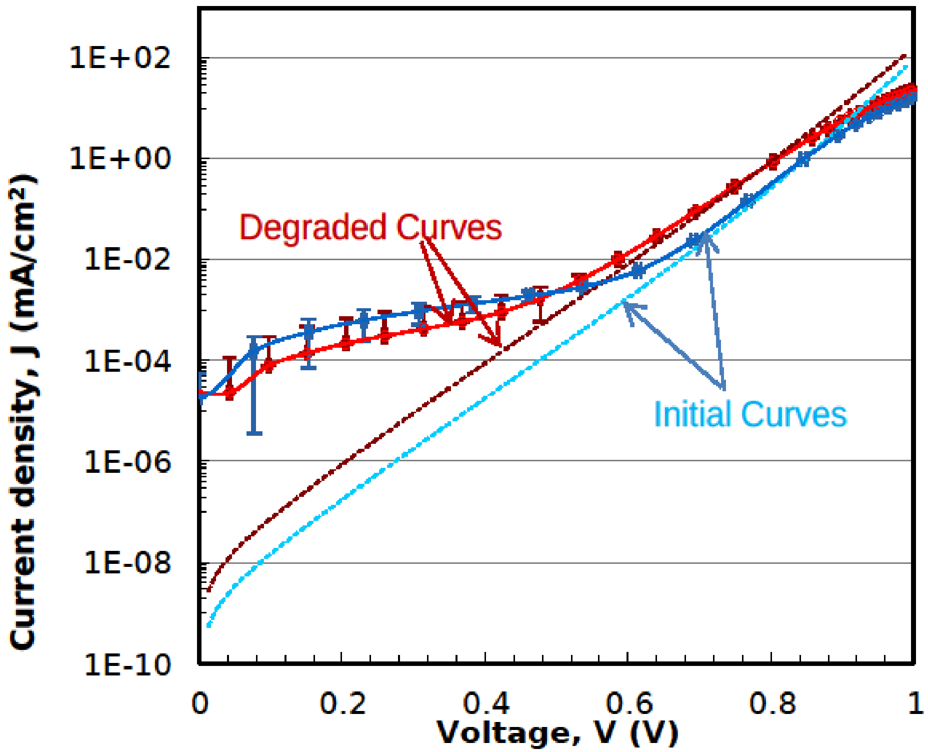

Figure 15: Dark forward J–V curves in the initial & degraded states for an experimental (continuous lines) T-Solar solar cell (1 cm²) and the simulated (dashed lines) ideal solar cell

- Ideal device → adjusts the experimental at middle voltages.
- Adding R_s →limits the current at high voltages.
- Shunt leakage → a current excess at low biases.
- Comparing ideality factor:

	n
Exp. initial state	1.72 ± 0.09
Sim. initial state	1.61
ϵ (%)	6.25
Exp. degraded state	1.88 ± 0.08
Sim. degraded state	1.70
ϵ (%)	9.63

CiTIUS

Solar Cell Simulation (III)

Results under dark conditions

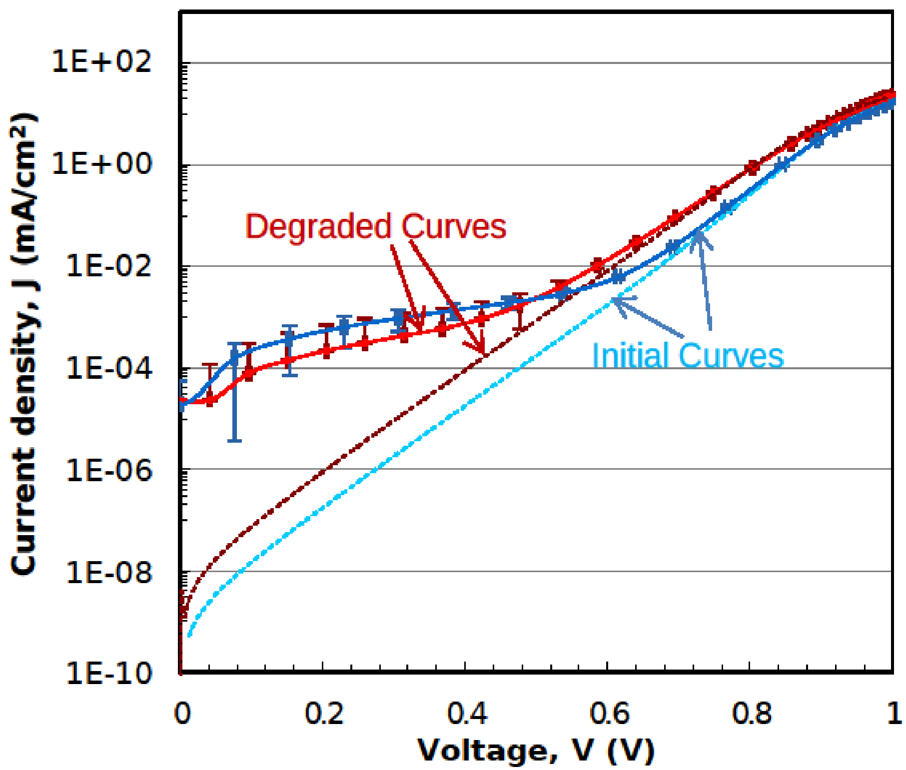

Figure 16: Dark forward J–V curves in the initial & degraded states for an experimental (continuous lines) T-Solar solar cell (1 cm^2) and the simulated (dashed lines) solar cell, including R_s

- Ideal device → adjusts the experimental at middle voltages.
- Adding R_s →limits the current at high voltages.
- Shunt leakage → a current excess at low biases.
- Comparing ideality factor:

	n
Exp. initial state	1.72 ± 0.09
Sim. initial state	1.61
ϵ (%)	6.25
Exp. degraded state	1.88 ± 0.08
Sim. degraded state	1.70
ϵ (%)	9.63

CiTIUS

Solar Cell Simulation (III)

Results under dark conditions

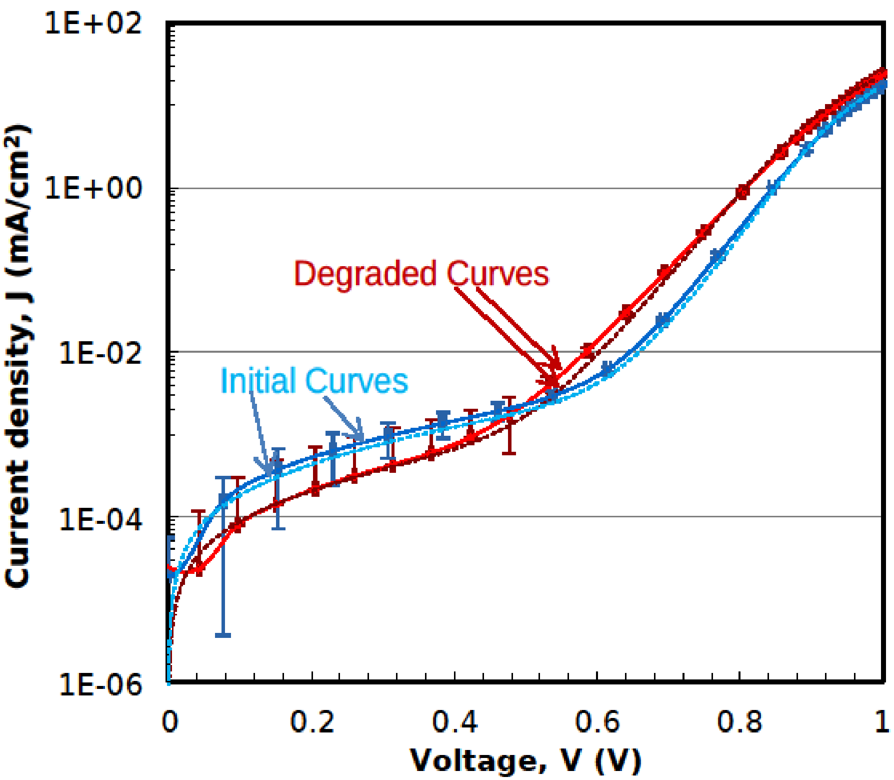

Figure 17: Dark forward J–V curves in the initial & degraded states for an experimental (continuous lines) T-Solar solar cell (1 cm^2) and the simulated (dashed lines) solar cell, including R_s and R_{sh}

- Ideal device → adjusts the experimental at middle voltages.
- Adding Rs →limits the current at high voltages.
- Shunt leakage → a current excess at low biases.
- Comparing ideality factor:

	n
Exp. initial state	1.72 ± 0.09
Sim. initial state	1.61
ϵ (%)	6.25
Exp. degraded state	1.88 ± 0.08
Sim. degraded state	1.70
ϵ (%)	9.63

Solar Cell Simulation (IV)

Results under light conditions

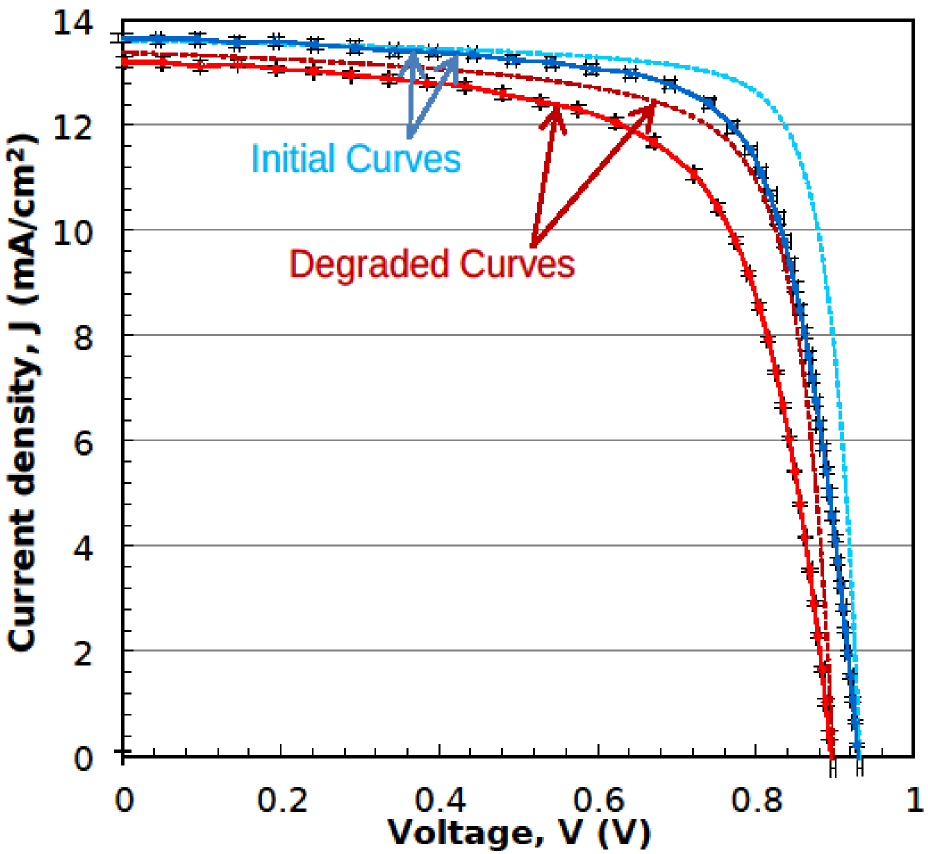

Figure 18: Illumination J–V curves in the initial & degraded states, for an experimental (continuous lines) T-Solar solar cell (1 cm²) and the simulated (dashed lines) ideal solar cell

- Ideal pin structure→ more FF.
- R_s dominant at high voltages.
  - Efficiency was reduced from 10.14% to 9.63% (initial state) and from 8.94% to 8.50% (degraded state).
- Adding as well shunt leakage:
  - Cell efficiency decreased from and 9.63% to 9.42% in the initial state, and from 8.50% to 8.10% in the degraded state.

CiTIUS

Solar Cell Simulation (IV)

Results under light conditions

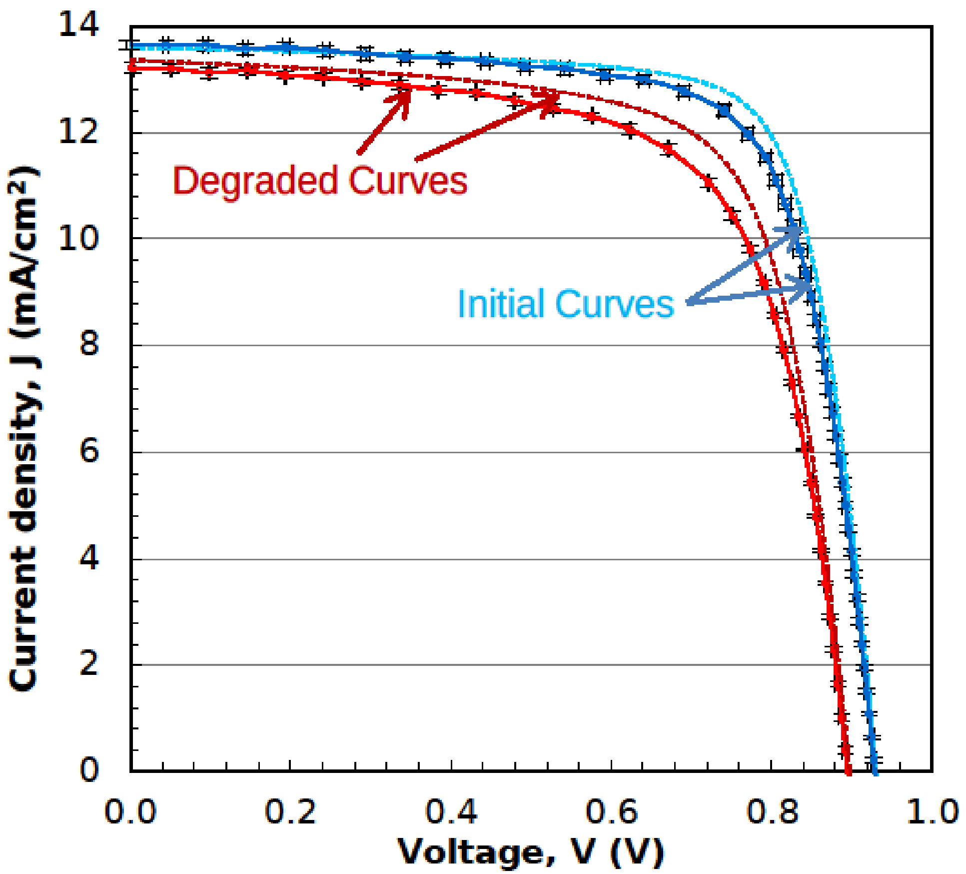

Figure 19: Illumination forward J–V curves in the initial & degraded states for an experimental (continuous lines) T-Solar solar cell (1 cm²) and the simulated (dashed lines) solar cell, including R_s

- Ideal pin structure→ more FF.
- R_s dominant at high voltages.
  - Efficiency was reduced from 10.14% to 9.63% (initial state) and from 8.94% to 8.50% (degraded state).
- Adding as well shunt leakage:
  - Cell efficiency decreased from and 9.63% to 9.42% in the initial state, and from 8.50% to 8.10% in the degraded state.

CiTIUS

Solar Cell Simulation (IV)

Results under light conditions

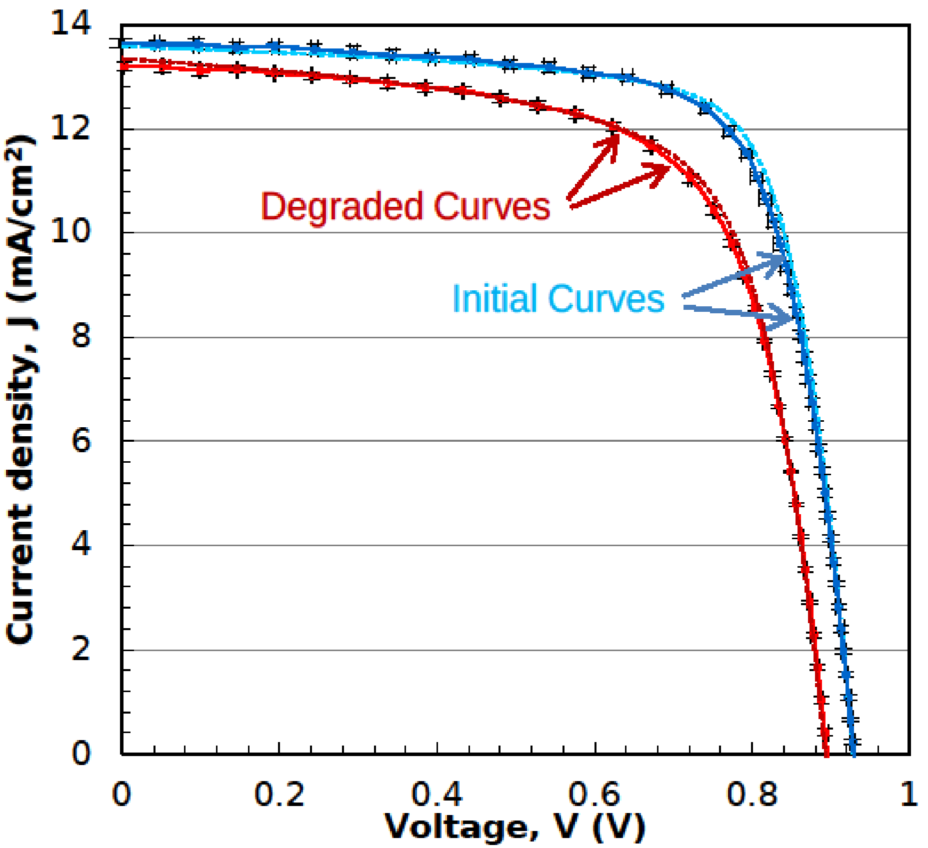

Figure 20: Illumination forward J–V curves in the initial & degraded states for an experimental (continuous lines) T-Solar solar cell (1 cm^2) and the simulated (dashed lines) solar cell, including R_s and R_{sh}

- Ideal pin structure→ more FF.
- R_s dominant at high voltages.
  - Efficiency was reduced from 10.14% to 9.63% (initial state) and from 8.94% to 8.50% (degraded state).
- Adding as well shunt leakage:
  - Cell efficiency decreased from and 9.63% to 9.42% in the initial state, and from 8.50% to 8.10% in the degraded state.

CiTIUS

Solar Cell Simulation (IV)

Conclusions

- With all the input models, experimental data and performed parameterizations, we obtained a simulation that reproduces well the current voltage characteristics of the studied device.
- We added, an ohmic resistance in the front contact, as R_s and (assuming Al diffusion) we simulated a microscopic pip structure, as R_{sh}; obtaining good agreement. This type of adjustment of both curves at dark and light conditions was not done before.
- An absolute 1% of the efficiency is lost due to the effect of R_s and shunt leakage, thus the importance of reducing this defect's size.
- Due to the influence of phosphorus in the Al diffusion, we suggest to improve chamber cleaning, or try oder n-type doppants.

Development of VFSR measurement system

Traditional SR Measurement System

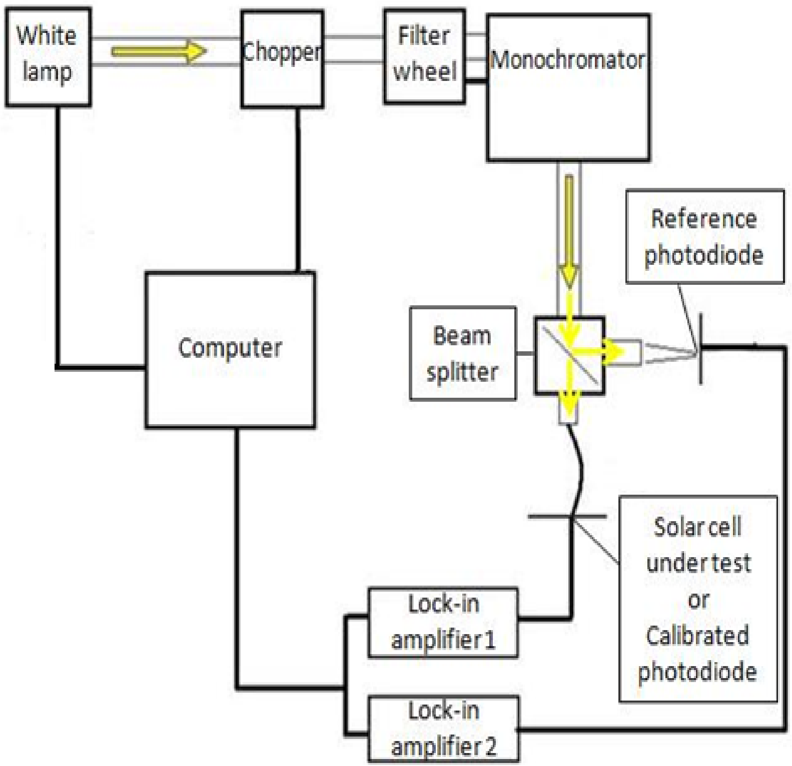

Figure 21: Diagram of a traditional SR measurement system

- Traditional SR measurements:
  - On lab scale, monochromator light, lock-in amplifier to measure small currents.
  - Time consuming method, ≈15 min. → not suitable for J_{sc} mappings in large area modules.
- DSR: I_{ref} vs. I_{cell} illuminated simultaneously by the same light source.
- Determination of the calibration factor (F(l)) & SR:

$$R_{cell}(\lambda) = \frac{I_{cell}(\lambda)}{I_{ref}(\lambda)} \cdot F(\lambda) \cdot R_c(\lambda), \quad where\ F(\lambda) = \frac{I_{ref}(\lambda)}{I_c(\lambda)} \qquad (1)$$

$$I_{sc} = \int_{\lambda_i}^{\lambda_f} G(\lambda) \cdot R(\lambda) \cdot S \cdot d\lambda \qquad (2) \qquad EQE = \frac{R}{q} \cdot \frac{h\,c}{\lambda} \qquad (3)$$

CiTIUS

Development of VFSR measurement system (II)

Characteristics

- VFSR measurement system:
  - SR measurement in the range of seconds.
  - Simultaneous light generation by LEDs operating at different frequencies.
  - FFT analysis to extract current generated by each LED.

White lamp ⟷ LEDs

Lock-in amplifier ⟷ Current meter (sensitive & fast)

CiTIUS

Development of VFSR measurement system (III)

Applications and Objectives

APPLICATION

- Increase the number of measurements on small test solar cells and modules.
- Combining the VFSR with an XY displacement system → SR mappings.
- In-line diagnosis to identify possible process errors.

OBJECTIVE

- Optimization of deposition process to increase the overall module current.

CiTIUS

Development of VFSR measurement system (IV)

Fast Fourier Transform

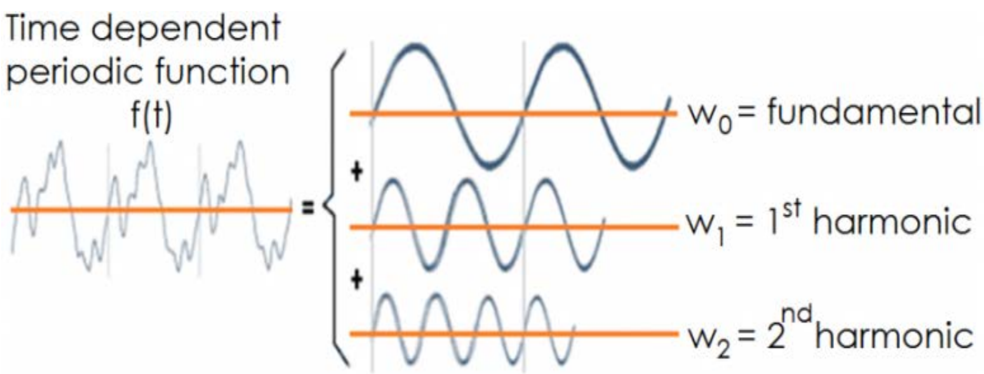

Figure 22: Periodic signals after Fourier analysis is decompound into its fundamental and harmonics

- Fundamental tool of the VFSR system.
- Using the Fourier transform a periodic signal f(t) can be expressed as a sum of different sinusoidal signals with frequencies $w=nw_0$.
- When n=1 we talk about the fundamental frequency.
- While n=2,3,4... are the harmonics.
- FFT is a fast way to calculate the Fourier transform of a sampled signal.

CiTIUS

Development of VFSR measurement system (V)

Fast Fourier Transform (II)

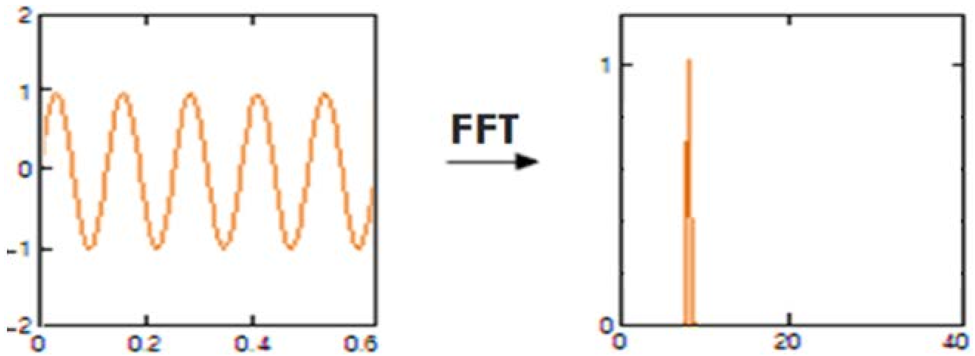

Figure 23: Sinusoidal signal in the time domain and its equivalence in the frequency domain after performing FFT

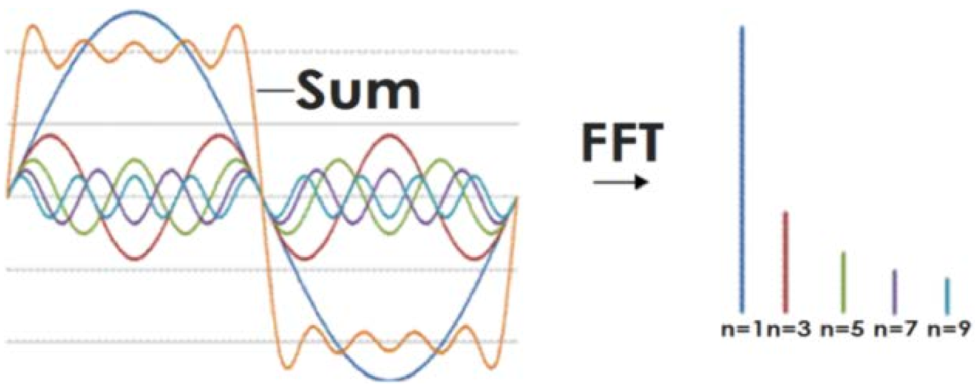

Figure 24: Periodic square signal and its harmonics both in the time and frequency domain (the later after FFT analysis)

- A sinusoidal signal equals, in the frequency domain, to a pulse placed at the frequency of the signal.

- An square signal, in the frequency domain equals to a train of pulses placed at the impair multiples of the frequency of the original signal. The amplitude of this pulses is modulated by an exponential.

Development of VFSR measurement system (VI)

Electrical characterization of LEDs

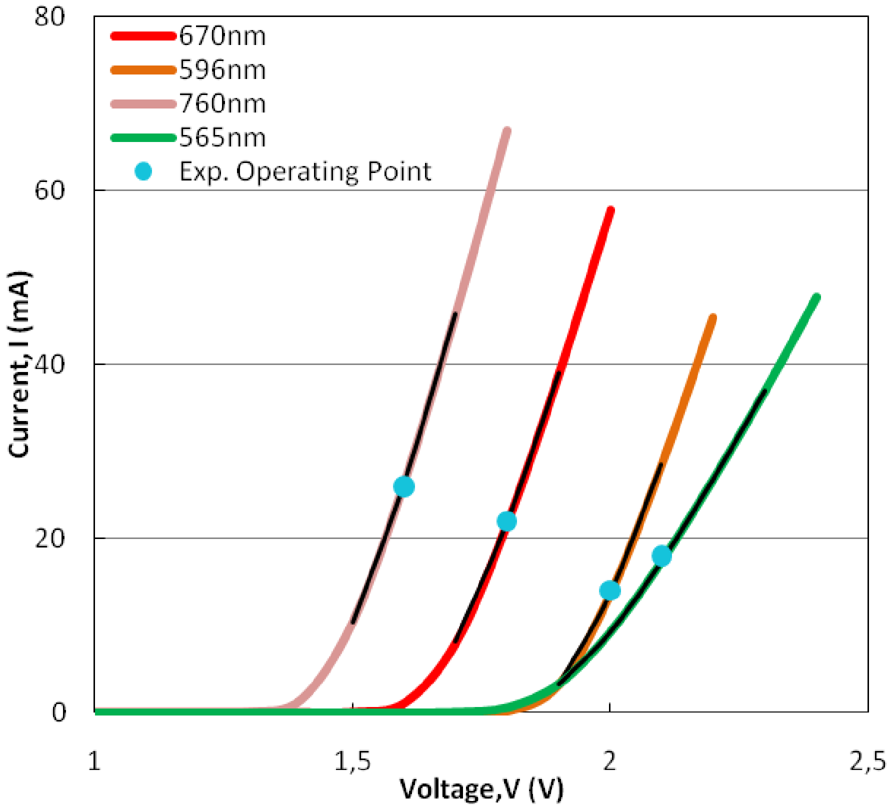

Figure 25: Experimental I-V curve and DC bias point for 4 representative LEDs. The black lines indicate the AC amplitude

- I-V curves of representative LEDs.
- DC operating point.
- AC range.
- LEDs are always on, they just modulate the intensity of their light.

CiTIUS

Development of VFSR measurement system (VII)

Optical characterization of LEDs

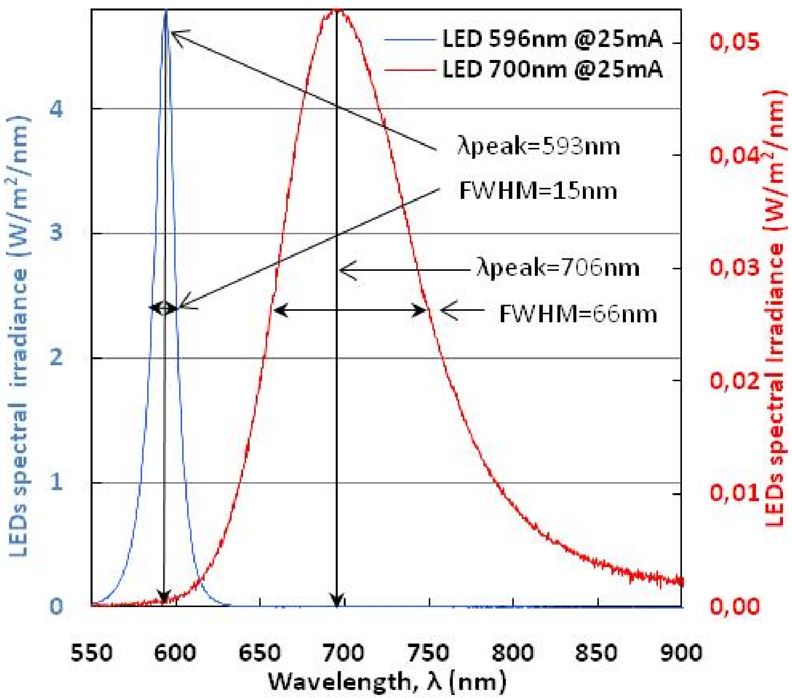

Figure 26: Peak wavelength (λ_{peak}) and FWHM for a LED with narrow band width & for a LED with wide band width

- To minimize the measurement error:
  - Exact determination λ_{peak} .
  - LEDs with narrow band width.

Development of VFSR measurement system (VIII)

Optical characterization of LEDs

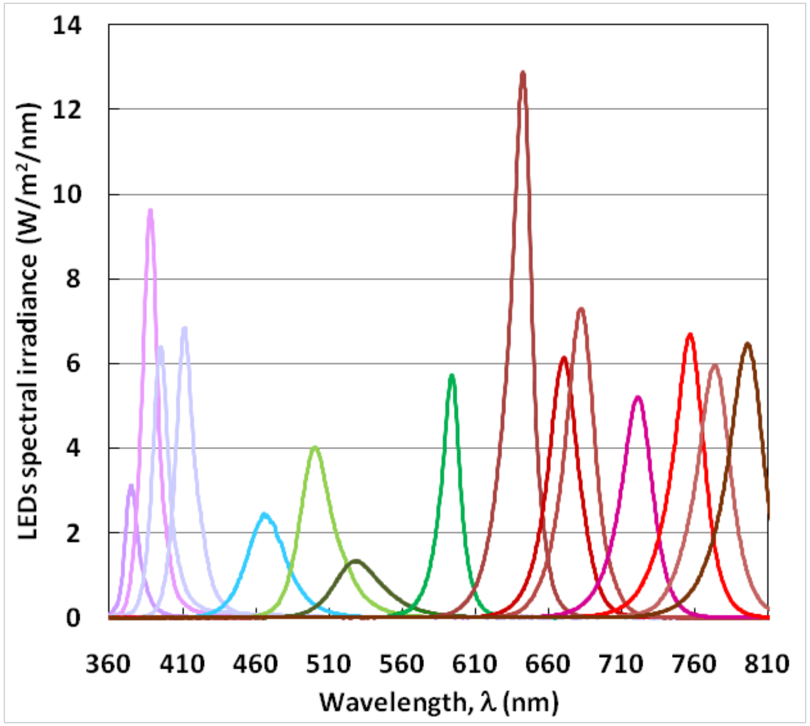

Figure 27: Experimental spectral irradiance of the 16 selected LEDs

- Individual spectra for the 16 selected LEDs.
- Optimization of illumination with LEDs ongoing.
- We have found LEDs for covering gaps.

CiTIUS

Development of VFSR measurement system (IX)

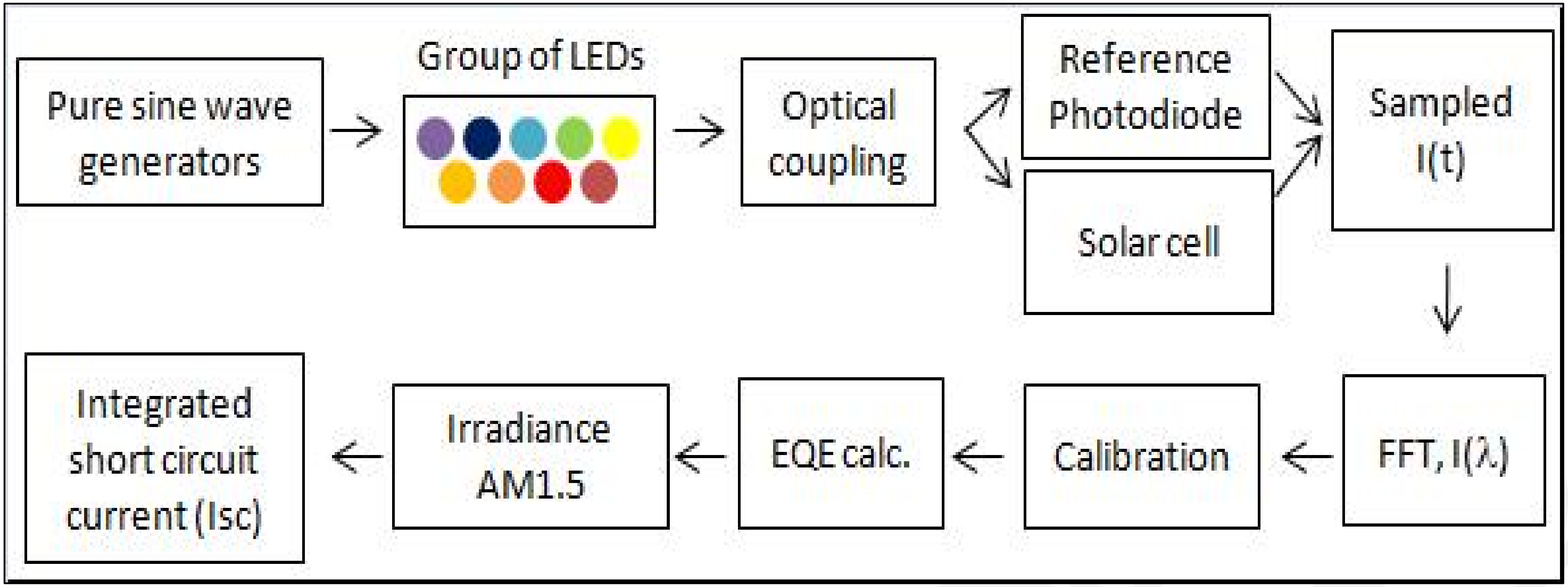

Figure 28: Diagram of the VFSR measurement system

CiTIUS

Development of VFSR measurement system (X)

Results

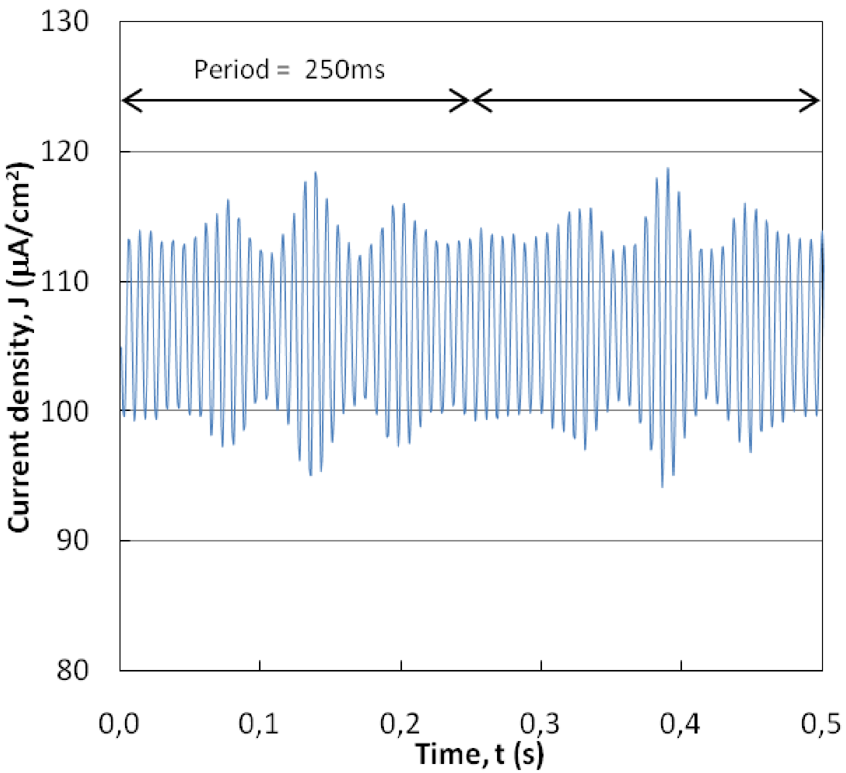

Figura 29: Time dependent current density curve presents repetition period of 250 ms

- Current meter with very high sample rate.
- Sampled J(t) curve of a 1cm^2 solar cell.
- Measurement of the J_{cell} in a few seconds.

Development of VFSR measurement system (XI)

Results (II)

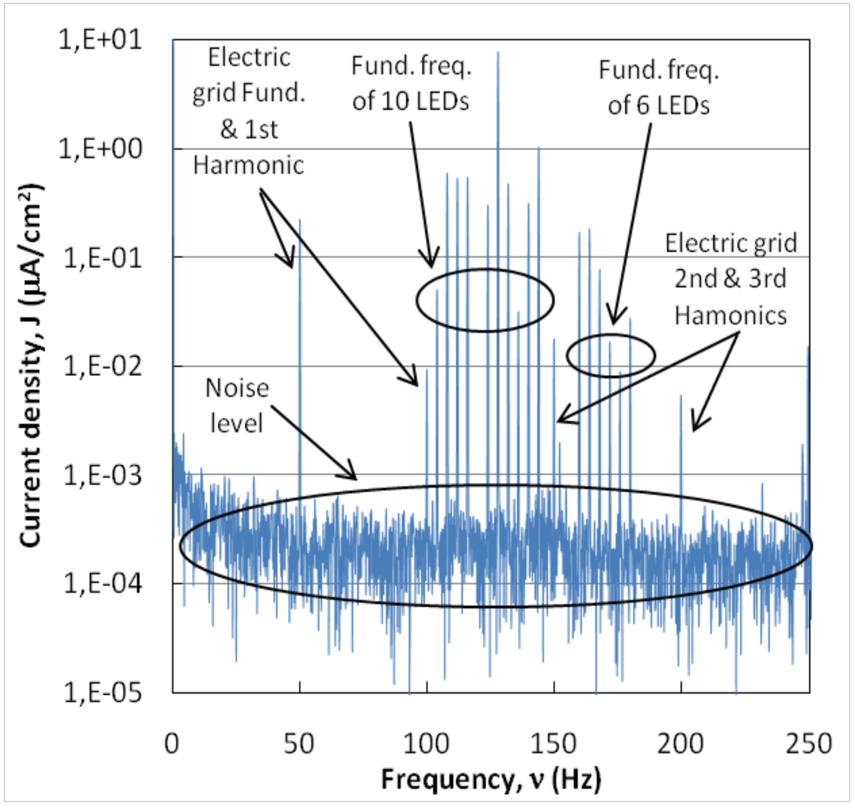

Figura 30: Current density curve in the frequency domain as resulting from FFT analysis

- Current density distribution in the frequency domain.
- Signal to noise ratio ≈2-4 orders of magnitude.
- Signal to noise ratio is objective of further improvements.
- Measurement analysis done with the peak current of the n_{fund}.

CiTIUS

Development of VFSR measurement system (XII)

Results (III)

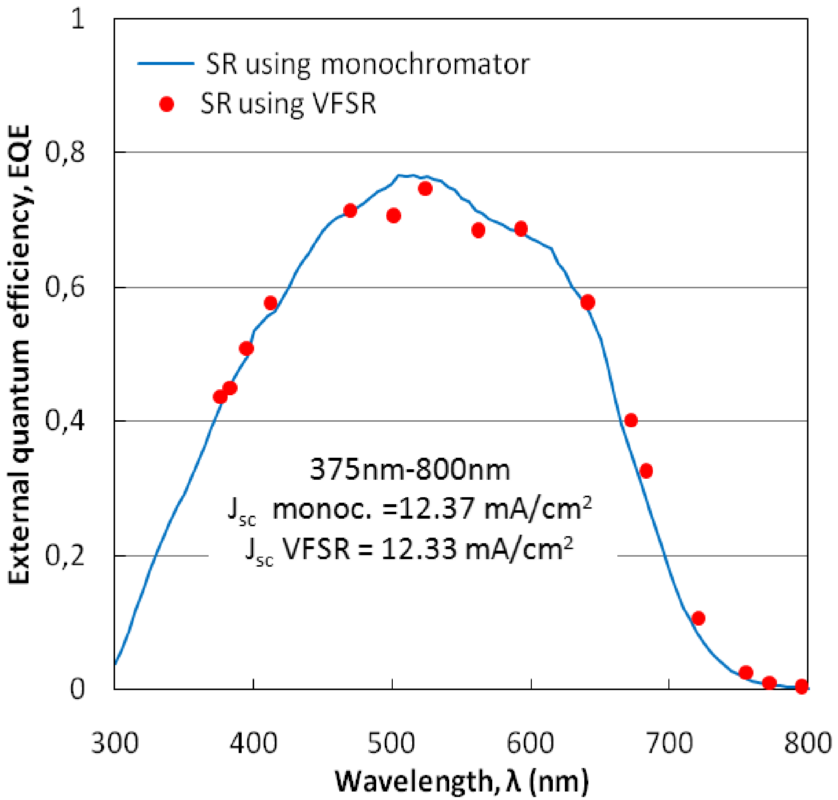

Figure 31: The difference between the J_{sc} determined with the traditional equipment and the VFSR is 0.26%

- $EQE_{traditional}$ vs. EQE_{VFSR}.
- For most of the points small deviation.
- Further optimization of LEDs operation will improve.
- Near UV wavelength range.
- IR wavelength range.

Development of VFSR measurement system (XII)

Conclusions

- SR measurements of a-Si:H solar cells in about 15 s.
- Careful characterization of the implemented LEDs is necessary.
- Precision of the measurement better than 1% in the J_{sc} calculation. It will be still improved.
- The performance of mapping experiments on modules is under investigation.
- Further improvement of the equipment is possible in the short wavelengths range.
- Up-grading of the equipment to ≈1000nm for tandem structures (a-Si/mc-Si), in progress.

CiTIUS

Thank you for your attention